Direct measurement of index of refraction in the extreme-ultraviolet wavelength region with a novel interferometer

Chang Chang,* Erik Anderson, Patrick Naulleau, Eric Gullikson, Kenneth Goldberg, and David Attwood*

Center for X-Ray Optics, Lawrence Berkeley National Laboratory, Berkeley, California 94720

Received November 21, 2001

To the best of our knowledge, the first direct measurement of the dispersive part of the refractive index is performed at extreme-ultraviolet (EUV) wavelengths, where absorption is higher as compared with hard-x-ray and visible wavelengths. A novel diffractive optical element that combines the functions of a grating and a zone plate is fabricated with Fourier optical techniques and employed here for the first time at EUV/soft-x-ray wavelengths. Both the real and the imaginary parts of the complex refractive indices are measured directly by this technique without recourse to Kramers–Kronig transformations. Data for Al and Ni in the vicinity of their L and M edges, respectively, are presented as first examples of this technique. © 2002 Optical Society of America

OCIS codes: 160.2120, 120.3180.

Refractive indices, $n(\omega) = 1 - \delta(\omega) + i\beta(\omega)$, in the extreme-ultraviolet (EUV) wavelength region are complex and highly absorptive and have strong wavelength (photon energy) dependence.[1] The absorptive part $\beta(\omega)$ of the refractive index at EUV wavelengths is well tabulated by photoabsorption measurements. However, the real (dispersive) part of the refractive index, $\delta(\omega)$, at EUV wavelengths is less accurately known. Interferometry, which can provide independent measurements of δ and β, is difficult in the EUV/soft-x-ray (SXR) regions because of high absorption by the many atomic resonances and the lack of high optical quality beam splitters. Joyeux *et al.*[2] had some success using an interferometer based on a bimirror reflective splitter but were limited by the trade-off between throughput and spectral resolution. Bonse and Hart[3] were successful at significantly higher photon energies, where $\beta/\delta << 1$, using crystal diffraction techniques. At present, in the EUV/SXR region, knowledge of δ is determined either indirectly from a Kramers–Kronig transformation of the imaginary (absorptive) part, $\beta(\omega)$,[4–7] or by least-squares fitting of Fresnel coefficients obtained from reflectance measurements.[7,8] Neither of these methods provides an independent measurement of $\delta(\omega)$. The $\delta(\omega)$ values obtained from the Kramers–Kronig relation depend entirely on the $\beta(\omega)$ values. Because the Kramers–Kronig relationship requires a wide range of spectrum of $\beta(\omega)$ for one to obtain each point $\delta(\omega)$ on the spectrum, errors in $\beta(\omega)$, especially near absorption edges, affect the accuracy of the resultant $\delta(\omega)$ values. The accuracy of $\delta(\omega)$ values determined from reflectance experiments are sensitive to surface roughness, chemistry, and contamination and to the fact that the accuracy of this fitting depends strongly on β/δ and works well only for energies with $\beta/\delta \ll 1$.

Here, we present an amplitude-division transmission interferometer that can be used to measure both the dispersive and the absorptive parts of the refractive index independently by determining the phase shift and the visibility of interferograms. Because the determination of δ directly from the phase shift is independent of β, this interferometer can measure δ across the absorption edges without being affected by sharp spectral variations of the β value. In addition, the sample is probed in transmission at normal incidence, and thus it is less sensitive to errors associated with surface roughness, chemistry, and contamination than are reflectance measurements, assuming that the thickness of the sample is much greater than that of the surface layer.

The interferometer used for the measurements is shown conceptually in Fig. 1. The size of the pinhole, 5 μm, is chosen to be smaller than the coherence area of the beam,[11] guaranteeing spatially coherent illumination of the interferometer. In concept, the pinhole-diffracted beam then propagates through a binary transmission grating, which serves as a beam splitter, followed by a zone plate lens that is used to focus the beams to the sample plane. As actually used, the grating and the zone plate are combined for improved efficiency into a single diffractive element that is discussed below, following Eq. (1).

The sample mask, consisting of side-by-side window pairs, is placed at the back focal plane of the zone plate. The window pairs consist of two 5 μm $\times$ 5 μm cross-sectioned openings. Reference window pairs are free of test material, whereas other pairs have

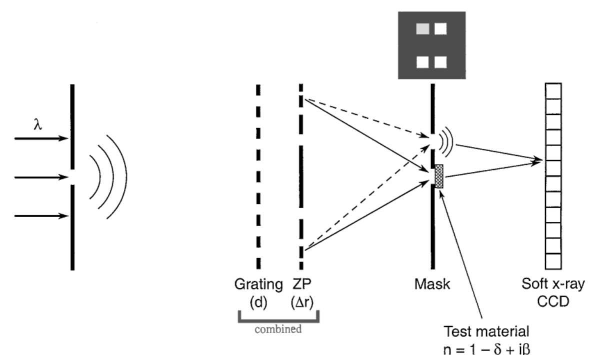

Fig. 1. EUV interferometer for direct $n(\omega)$ measurement.

 © 2002 Optical Society of America

one window coated with test material. In taking the data, we first align a reference window pair to the two side-by-side first-order focal beam spots and record a reference interferogram. We then move the sample mask to illuminate a window pair in which one side contains test material and record the test interferogram. By introduction of the test material into one arm of the interferometer, the fringes of the interferogram shift as a result of the refractive properties of the material, essentially a path integration of $\delta(\omega)$. Additionally, the visibility of the interferogram is reduced because of absorption. The interferograms are recorded on a backthinned EUV-sensitive CCD camera. The complex index of refraction is determined by comparison of these two interferograms for fringe shift and visibility change, which are directly related to δ and β, respectively.

A Fourier transform method[9,10] is used to extract both the phase shift and visibility from the interferograms. The extracted values are averaged over the full area of the interference pattern. The phase shift, ϕ, is simply the difference between the two independently reconstructed phase maps from the interferograms. The value of δ is determined by $\phi = (2\pi/\lambda)t\delta$, where λ is the wavelength and t is the sample thickness.

The relative optical intensities of the two beams after they propagate through the sample mask are related to the observed visibility of the interferogram by $V = 2\sqrt{\alpha}/(1 + \alpha)$, where α is the relative intensity of the beams after they propagate through the sample. The value of β is obtained from $\alpha = \exp(-{}^{4\pi}/_{\lambda}\,\beta t)$.

The use of two sequential diffractive elements (the grating and the zone plate), each of which has a theoretical efficiency to first order of $1/\pi^2$, limits the overall efficiency of the interferometer. This efficiency can be significantly improved by consolidation of the functionalities of the grating and the zone plate into a single diffractive optical element through a bitwise XOR operation.[11]

The two optical elements used in this XOR pattern, a 50% duty-cycle binary amplitude grating of period d, and a 50% duty-cycle binary amplitude zone plate of diameter D and outermost zone width Δr, can be represented by $G(x, y) = 1/2[1 + \mathrm{sgn}(\cos 2\pi x/d)]$ and $\mathrm{ZP}(x, y) = 1/2\{1 + \mathrm{sgn}[\cos \pi(x^2 + y^2)/\Delta r(D - \Delta r)]\}$, respectively.[12] Expanding these two patterns in their respective Fourier series and noting that the XOR pattern of the grating and the zone plate can be expressed as $\mathrm{XOR}(x, y) = G(x, y) + \mathrm{ZP}(x, y) - 2G(x, y)\mathrm{ZP}(x, y)$, we have

$$\mathrm{XOR}(x,y) = \frac{1}{2} - 2\left[\sum_{\substack{m=-\infty\\ m\neq 0}}^{\infty} \frac{\sin(m\pi/2)}{m\pi} \exp\left(-i\,\frac{2m\pi x}{d}\right)\right] \times \left\{\sum_{\substack{n=-\infty\\ n\neq 0}}^{\infty} \frac{\sin(n\pi/2)}{n\pi} \exp\left[-i\,\frac{n\pi(x^2+y^2)}{\Delta r(D-\Delta r)}\right]\right\}. \quad (1)$$

Examining the first-order terms, i.e., $(m, n) = (\pm 1, 1)$, we find that each has an efficiency that is given by the square of its coefficient $[2(1/\pi)(1/\pi)]^2 = 4/\pi^4$, which is a factor-of-4 increase in optical throughput compared with that of a separate grating and zone plate. Since the membranes on which these optical elements are fabricated have finite absorption, there is an additional gain of efficiency that is due to the fact that only one membrane is required.

This combined diffractive element, when it is illuminated by a uniform wave front, has the interesting property that it produces two symmetric off-axis focal spots, $(m, n) = (\pm 1, 1)$, at the back focal plane of the zone plate. This can be seen by multiplication of the two exponentials in Eq. (1) and completion of the square for x terms. The separation of these two beam spots is determined by $\Delta x \approx 2 \sin^{-1}(\lambda/d)(\Delta r D)/\lambda = 2\Delta r D/d$. Note that this separation is independent of wavelength λ. Thus, as the wavelength is varied for spectral determinations of δ and β, the focal length (the distance from the XOR pattern to the sample mask) varies but the lateral separation of the two beam spots remains fixed. Therefore, the index of refraction as a function of wavelength can be obtained simply by translation of the sample mask along the optical axis.

This experiment is performed at undulator beamline 12.0 of the Advanced Light Source.[13] Undulator radiation provides the required EUV photon flux and, with pinhole spatial filtering, the spatial coherence required for the interferometric experiments. The beamline monochromator provides a spectral resolution of $\lambda/\Delta\lambda = 1100$. As described above, a single XOR diffractive element combining a grating ($d = 16$ μm) and a zone plate ($D = 400$ μm, $\Delta r = 0.2$ μm) is used for optimum efficiency. This new diffractive element is fabricated with electron-beam patterning and nanofabrication techniques.[14] The separation of the two beam spots at the back focal plane is $\Delta x = 10$ μm.

The sample mask is also fabricated by electron-beam lithography on a 100-nm-thick Si_3N_4 membrane. The thickness of the Si_3N_4 membrane is relatively uniform over the 10-μm separation of the two beam spots. The sample is prepared by evaporation of the test material onto the nitride membrane. The thickness of the test material is measured by both a profilometer and a spectral reflectivity system to an accuracy ± 1 nm.

Measured δ and β values for 67.0 $\pm$ 0.1-nm-thick Al are shown in Fig. 2 by error bars. The results obtained with this interferometer resolve the fine Al L-edge structure, i.e., the L_3 edge at 72.7 eV and the L_2 edge at 73.1 eV, in both δ and β. Moreover, it is also evident that the shapes of the δ and β curves, although they are determined independently, are closely related. The sharpest increase in β occurs at 72.7 eV, which coincides exactly with the dip of the δ curve at the L_3 edge. Furthermore, the sharp increase of β at 73.1 eV also coincides exactly with the dip of the δ curve at the L_2 edge. For comparison, the best available data for Al refractive indices are also shown (without error bars),[7] where the δ value is obtained by Kramers–Kronig transformations of β values over a wide spectrum. The two data sets agree fairly well for both δ and β.

Measured δ and β values for Ni of 20.6 $\pm$ 0.1-nm thickness are shown in Fig. 3 by error bars. The

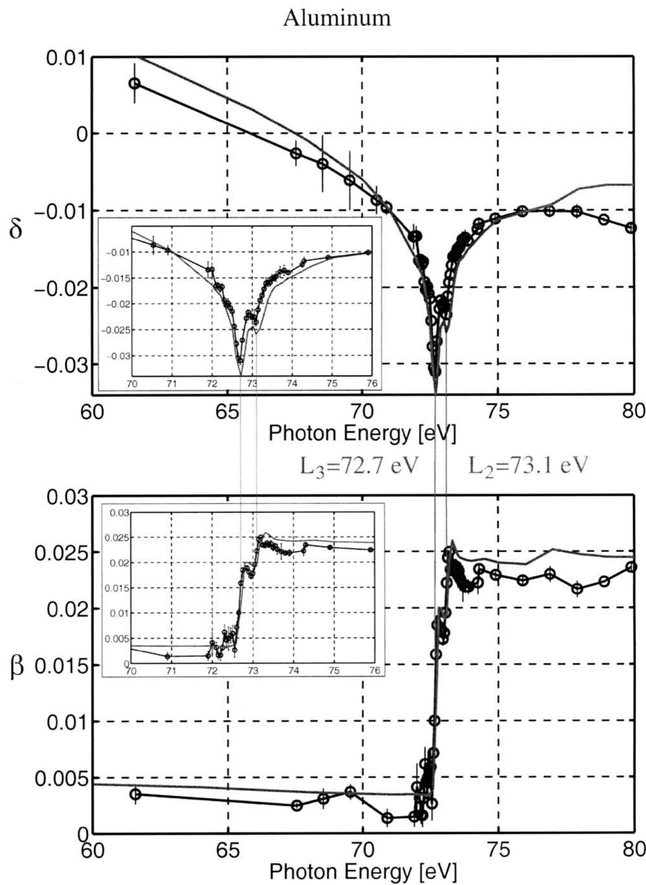

Fig. 2. Al data (with error bars) are shown with the current standard.

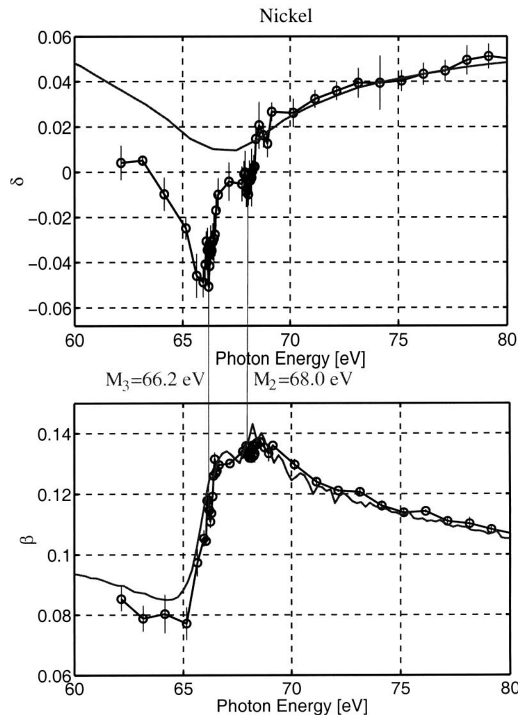

Fig. 3. Ni data (with error bars) shown with the current standard.

Ni M_3 edge at 66.2 eV is clearly resolved, and the δ and β values at this edge can be seen to be closely correlated. The error bars for the Ni data are slightly larger than those of the Al data, mainly because of the lower photon flux available in our experiment at the Ni M edge. Thus, longer exposure times were required, resulting in greater noise as a result of vibration. Improved accuracy will require increased system stability or increased optical throughput. The best available refractive index values of Ni are also shown (without error bars) for comparison.

The first direct measurement of the index of refraction at EUV wavelengths has been performed with interferometry. A new diffractive optical element based on Fourier optical techniques has been demonstrated in the interferometer for improved efficiency for the first time.

C. Chang's e-mail address is cnchang@lbl.gov.

*Department of Electrical Engineering and Computer Sciences, University of California, Berkeley, California 94720.

References

1. D. T. Attwood, *Soft X-Rays and Extreme Ultraviolet Radiation: Principles and Applications* (Cambridge U. Press, Cambridge, 1999).
2. D. Joyeux, F. Polack, and D. Phalippou, Rev. Sci. Instrum. **70,** 2921 (1999).
3. U. Bonse and M. Hart, Appl. Phys. Lett. **6,** 155 (1965).
4. H. Ehrenreich and H. R. Philipp, Phys. Rev. **128,** 1622 (1962).
5. H.-J. Hagemann, W. Gudat, and C. Kunz, J. Opt. Soc. Am. **65,** 742 (1975).
6. E. Shiles, T. Sasaki, M. Inokuti, and D. Y. Smith, Phys. Rev. B **22,** 1612 (1980).
7. R. Soufli, "Optical constants of materials in the EUV/soft x-ray region for multilayer mirror applications," Ph.D. dissertation (University of California, Berkeley, Berkeley, Calif., 1997).
8. W. R. Hunter, Appl. Opt. **21,** 2103 (1982).
9. C. Chang, P. Naulleau, E. Anderson, and D. Attwood, Opt. Commun. **182,** 25 (2000).
10. M. Takeda, H. Ina, and S. Kobayashi, J. Opt. Soc. Am. **72,** 156 (1982).
11. The XOR pattern is obtained first by pixelization of the binary grating and the zone plate. Each pixel is 1 for transmission and 0 for absorption. The two pixelized patterns are then overlapped and compared pixel by pixel, producing the resulting XOR pattern; i.e., at each pixel position, if the pixel values of the grating and the zone plate are the same (both 0's or both 1's), the value of the corresponding pixel on the XOR pattern is 0. Otherwise, the value of the corresponding pixel on the XOR pattern is 1.
12. J. W. Goodman, *Introduction to Fourier Optics*, 2nd ed. (McGraw-Hill, New York, 1996).
13. D. T. Attwood, P. Naulleau, K. A. Goldberg, E. Tejnil, C. Chang, R. Beguiristain, P. Batson, J. Bokor, E. M. Gullikson, M. Koike, H. Medecki, and J. H. Underwood, IEEE J. Quantum Electron. **35,** 709 (1999).
14. E. H. Anderson, D. L. Olynick, B. Harteneck, E. Veklerov, G. Denbeaux, W. Chao, A. Lucero, L. Johnson, and D. Attwood, J. Vac. Sci. Technol. B **18,** 2970 (2000).
15. E. Gullikson, http://www-cxro.lbl.gov/optical_constants/.